CONTRAST MEDIA & MOLECULAR IMAGING

Received: 20 July 2010, Revised: 10 September 2010, Accepted: 13 September 2010, Published online in Wiley Online Library: 29 December 2010

(wileyonlinelibrary.com) DOI:10.1002/cmmi.423

In vitro biomedical applications of functionalized iron oxide nanoparticles, including those not related to magnetic properties

Carmen Burtea[a], Sophie Laurent[a], Isabelle Mahieu[a], Lionel Larbanoix[a], Alain Roch[a], Marc Port[b], Olivier Rousseaux[b], Sébastien Ballet[b], Oltea Murariu[a], Gérard Toubeau[c], Claire Corot[b], Luce Vander Elst[a] and Robert N. Muller[a]*

Superparamagnetic iron oxide nanoparticles (SPION) are very promising contrast media, especially for molecular imaging, due to their superior NMR efficacy. They even have wider biomedical applications such as in drug and gene delivery, tissue engineering and bioseparation, or as sensitive biological nanosensors. By coupling them to affinity ligands, SPION can bind to drugs, proteins, enzymes, antibodies or nucleotides. For *in vitro* biomedical applications, the detection of molecular interaction is possible by using a diversity of systems capable of sensing the magnetic properties of these materials. The goal of the present work was to develop and validate various *in vitro* biomedical applications of ultrasmall superparamagnetic particles of iron oxide (USPIO), including some that are not related to their magnetic properties. USPIO coated with dextran, starch or bisphosphonate exposing carboxylate groups were synthesized and some of them were functionalized by conjugating various biomolecules, such as biotin, streptavidin and apoptosis, or VCAM-1 specific peptides. The *in vitro* biomedical applications assessed in the present work included: (1) the relaxometric measurement of antibody concentration, cell receptor expression, molecular interaction, and enzymatic activity in aqueous suspensions; (2) MRI visualization of cells and detection of molecular interaction in an ELISA system; (3) ELISA applications of USPIO derivatives; and (4) detection of specific biomolecules by histochemistry. Our results confirm that rapid and simple *in vitro* detection of a diversity of functionalized SPION with relevance in medicine is possible by the existing NMR techniques and by chemical staining reactions. The protocols can be applied to minimally prepared biological samples (e.g. whole blood, blood plasma or serum, cell suspensions, biopsies, histological preparations, etc.), and often do not need complicated systems of signal amplification. The use of SPION labeled compounds could furthermore contribute to cost reductions in the diagnosis and in patient care. Copyright © 2010 John Wiley & Sons, Ltd.

Keywords: functionalized iron oxide nanoparticles; contrast agents; molecular targeting; relaxometry; MRI; ELISA; Perls' iron staining; histochemistry

1. Introduction

The outstanding intrinsic contrast offered by magnetic resonance imaging (MRI) provides particularly detailed anatomical images that surpass in resolution those of any other clinical imaging techniques. Additionally, the contrast agents (CAs) used in MRI can improve the difference between normal and diseased tissues and thus the diagnosis of many diseases by increasing (in the case of positive agents like paramagnetic CAs) or decreasing (in the case of negative agents like superparamagnetic CAs) the signal intensity subsequent to the shortening of the proton relaxation times (i.e. T_1 and T_2) of the imaged organs and tissues (1). Although not so popular yet for clinical applications as positive agents, superparamagnetic iron oxide nanoparticles (SPION) are very promising contrast media (2), especially for molecular imaging (3,4), due to their superior NMR efficacy (i.e. relaxivity) (5). Furthermore, the applications of SPION are not limited only to MRI contrast (6), but are much wider, such as in the drug and gene delivery, tissue engineering and bioseparation (7), or as sensitive biological nanosensors (8,9), contributing thus to a breakthrough revolution in nanomedicine.

SPION are composed of magnetite (Fe_3O_4), maghemite (γFe_2O_3) or other ferrites, which have a large magnetic moment in the

* *Correspondence to: R. N. Muller, E-mail: Robert.Muller@umons.ac.be*

a *C. Burtea, S. Laurent, I. Mahieu, L. Larbanoix, A. Roch, O. Murariu, L. Vander Elst, R. N. Muller*
Department of General, Organic and Biomedical Chemistry, NMR and Molecular Imaging Laboratory, University of Mons, Avenue Maistriau 19, Mendeleev Building, B-7000 Mons, Belgium

b *M. Port, O. Rousseaux, S. Ballet, C. Corot*
Guerbet, Research Center, 16-24 rue Jean Chaptal, 93600 Aulnay-sous-Bois, France

c *G. Toubeau*
Laboratory of Histology, University of Mons, Pentagon – 1B, 6 Avenue du Champ de Mars, B-7000 Mons, Belgium

presence of a static external magnetic field (10,11). They are divided into two classes depending on their hydrodynamic particle size: those with a mean diameter greater than 50 nm (small particles of iron oxide, SPIO) and those with a smaller hydrodynamic diameter (ultrasmall SPIO, USPIO) (2). Recently, several other metals, such as cobalt oxide, spinel cobalt or manganese ferrite ($CoFe_2O_4$, $MnFe_2O_4$) (12,13), and even gadolinium oxide (14), have been used in various compositions. To prevent their destabilization and agglomeration and to render them stable in aqueous or biological media, SPION are coated with polymeric materials, such as dextran, carboxymethylated dextran, carboxydextran, starch, PEG, arabinogalactan, glycosaminoglycan, organic siloxane and sulfonated styrene-divinylbenzene (2,15). By coupling them to affinity ligands, SPION can function as sensitive biological nanosensors, being able to bind to drugs, proteins, enzymes, antibodies or nucleotides (6,9). For *in vitro* biomedical applications, the detection of molecular interaction has been possible by using a diversity of systems capable of sensing the magnetic properties of these materials, i.e. a superconductive quantum interference device (SQUID) (16,17), handheld magnetic readers (18), magneto-resistive detectors (19,20), MRI (21), relaxometry (22–24), and a chip-NMR biosensor (25).

The magnetic nanosensors have been used up to now to detect a diversity of biomolecules (e.g. oligonucleotides, proteins, small molecules, viruses) with a high sensitivity (i.e. in the femtomole range), as the existing NMR techniques make it possible to analyze minimally prepared, even turbid, samples since the magnetic relaxation is not influenced by the optical properties of the solution. The MRI systems even permit the sample screening in a high-throughput setting, which is a prerequisite for pharmaceutical research (9,21).

The binding of these magnetic nanosensors to their target leads to the formation of a molecular nanoassembly, which modifies in a sensitive and dose-dependent manner the transverse relaxation time (T_2) of the surrounding water molecules. In fact, the T_2 can be prolonged or decreased as a function of the size of the aggregate that is formed subsequent to the molecular interaction. If the superparamagnetic particle consists of an aggregate of several crystals of magnetite contained in a flake of polysaccharides, the transverse relaxivity is characterized by the sum of two terms: the first one is created by the individual grain of magnetite and the second one is produced by the aggregate itself considered as a large magnetic sphere. If the coating is cut by an enzyme, for instance, the particles agglomerate and the transverse relaxivity evolves with the size of the cluster. Initially, the relaxivity increases as the square of the radius of the cluster, according to the outer sphere theory. For larger aggregates, the relaxivity reaches a maximum and then decreases with its diameter (26). In fact, the outer sphere theory is no longer valid for particles with a large diameter, and relaxation gradually tends to that given by the static model theory valid for very big particles. In these intermediate conditions, a part of the phase shift of the proton spin experiencing the field of the particle is refocused by the spin echo sequence; the amount of the refocused proton spin magnetization increases with the cluster diameter. The measured transverse relaxation rate depends on the echo time and tends to zero for very large size particles.

The goal of the present work was to develop and validate various *in vitro* biomedical applications of USPIO, including some that are not related to their magnetic properties. To that aim, USPIO derivatives coated with dextran ($USPIO_{dx}$), bisphosphonate exposing carboxylate groups ($USPIO_{COOH}$) or starch ($USPIO_{Stch}$) were synthesized and some of them were functionalized by conjugating various biomolecules as follows: (a) $USPIO_{dx}$ functionalized with biotin ($USPIO_{dx}$-Bt) or streptavidin ($USPIO_{dx}$-Strp) (22); (b) $USPIO_{dx}$ conjugated to apoptosis-targeted peptide ($USPIO_{dx}$-R826) (27); and (c) $USPIO_{COOH}$ conjugated to apoptosis (R826 and E3) (27,28) or VCAM-1 (R832) (29) targeted peptides and rendered furtive with polyethylene glycol ($USPIO_{COOH}$-R826-PEG, $USPIO_{COOH}$-E3-PEG, $USPIO_{COOH}$-R832-PEG, respectively). The biomedical applications of the USPIO derivatives assessed in this work included: (1) the relaxometric measurement of antibody concentration, cell receptor expression and molecular interaction in aqueous suspensions; (2) the relaxometric evaluation of amylase activity subsequent to the hydrolysis of USPIO's starch coating; (3) MRI visualization of cells and detection of molecular interaction in an ELISA system; (4) ELISA applications of USPIO derivatives; and (5) detection of specific biomolecules by histochemistry.

2. Results and discussion

2.1. Relaxometric measurement of antibody concentration in biological samples

The present experiment is founded on the idea that $USPIO_{dx}$-Strp and $USPIO_{dx}$-Bt could be used to detect and eventually measure the IgG concentration in biological samples subsequent to the molecular interaction between these biological entities. The macromolecular assembly of IgG-Bt, $USPIO_{dx}$-Strp and $USPIO_{dx}$-Bt induced a significant increase in transverse relaxation rate (R_2) which was easily detected with a bench-top relaxometer (Fig. 1A). The addition of IgG-Bt (final concentrations in the incubation mixture: 0.01–1.8 μM) to the combined solution of $USPIO_{dx}$-Strp (10 μM) and $USPIO_{dx}$-Bt (40 μM) raised the paramagnetic R_2 (R_2^{para}) in a concentration-dependent manner (Fig. 1B–D), being positively correlated with IgG concentration ($r^2 = 0.980$; Fig. 1C). The results in these figures are represented as a normalized R_2 (R_2^{Norm}), which was calculated by subtracting the R_2 of the combined solution of $USPIO_{dx}$-Strp and $USPIO_{dx}$-Bt from that of the test samples. The background R_2 does not significantly change during 1 h of incubation at 37 °C: $T_{0\ min} = 4.73\ s^{-1}$; $T_{30\ min} = 4.18\ s^{-1}$; $T_{60\ min} = 4.07\ s^{-1}$. The results were stable in time (Fig. 1B) and the method was highly sensitive to IgG-Bt concentrations as low as 10 nM. At low IgG-Bt concentrations, the relationship with R_2 was linear ($r^2 = 0.996$) and the calibration curve (Fig. 1D) could be used to quantify the antibody in solution or other biomolecules recognized by it.

2.2. Relaxometric measurement of cell receptor expression

The $USPIO_{dx}$-Strp and $USPIO_{dx}$-Bt interaction was also used to quantify the expression of T-cell receptor (CD3) by Jurkat T lymphocytes (Fig. 1E). For this purpose, the cells were incubated with biotinylated anti-CD3 antibody, and this last one was then detected by relaxometry after incubating various numbers of cells (2×10^6 to 0.15×10^6) with a constant concentration of $USPIO_{dx}$-Strp (10 μM) and $USPIO_{dx}$-Bt (40 μM). A very good correlation ($r^2 = 0.995$) was observed between the number of cells expressing the T-cell receptor and the measured R_2^{Norm}, which was calculated by subtracting the R_2 of the cells incubated with USPIO derivatives in the absence of anti-CD3 antibody from that of each test sample. The limit of receptor detection is in the picomolar order (2.5×10^{-10} M) if we consider 10^5 receptors per cell and 1.5×10^5 cells per 100 μl.

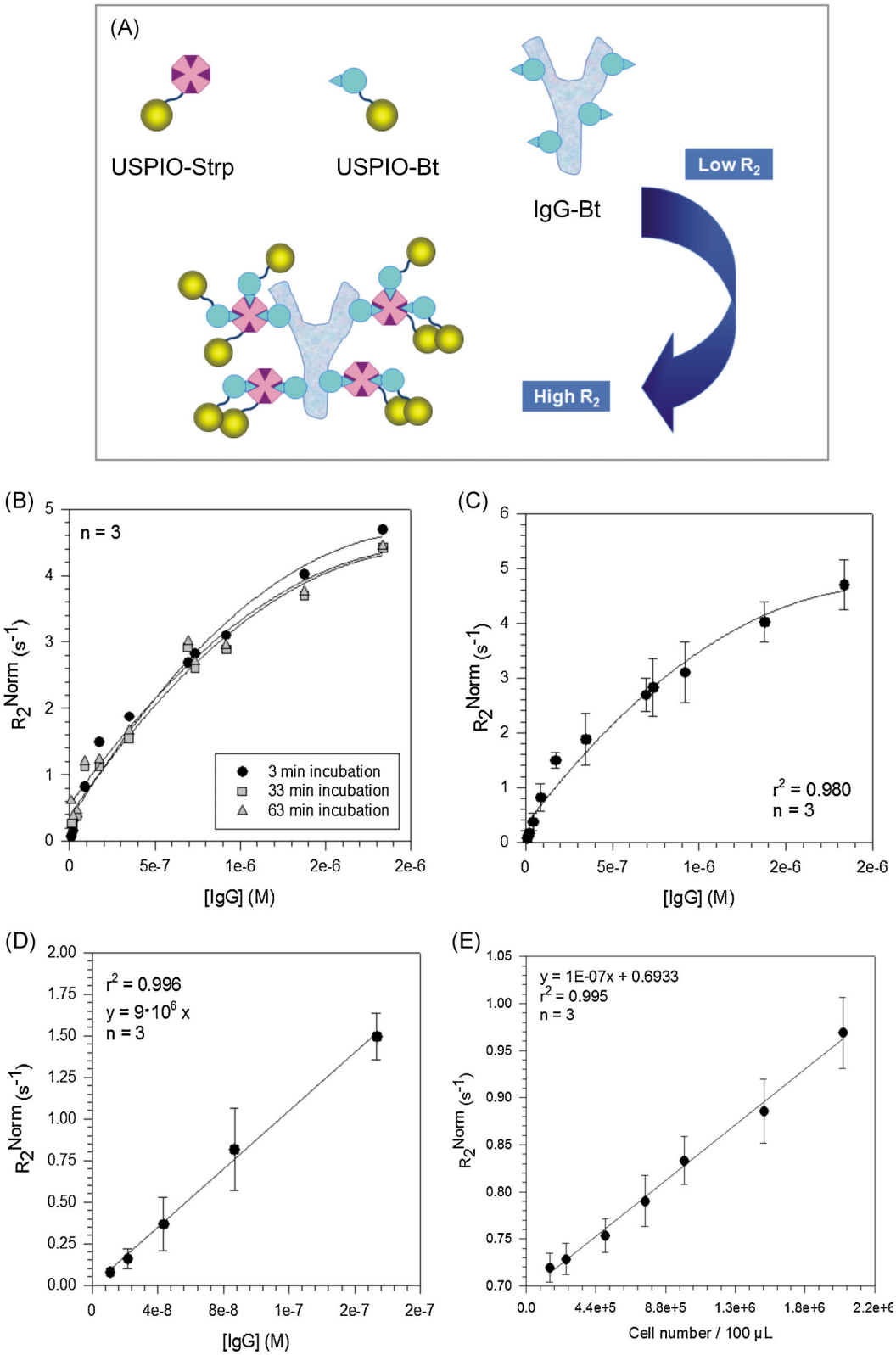

Figure 1. Interaction of $USPIO_{dx}$-Strp and $USPIO_{dx}$-Bt with IgG-Bt measured in solution by relaxometry at 60 MHz and 37 °C. The interaction between these molecular entities is associated with an increase of the transverse relaxation rate as it is schematically represented in (A). The concentration of iron oxide nanoparticles in the solution was maintained constant, while that of IgG-Bt varied from 0.01 to 1.8 µM. The R_2^{Norm} was measured after different times of incubation showing reproducibility (B). An incubation time of 3 min was sufficient to measure the molecular interaction and the R_2^{Norm} was reproducible between measurements, being proportional to IgG-Bt concentration (C). In the low concentration range of IgG-Bt, the curve is linear and could be used to quantify molecules (i.e. proteins) in solution (D). $USPIO_{dx}$-Strp and $USPIO_{dx}$-Bt were also used to detect biotinylated antibodies bound to T-cell receptor expressed by Jurkat T-lymphocytes showing a good correlation with the cell number in the sample (E). The results are represented as means ± SEM.

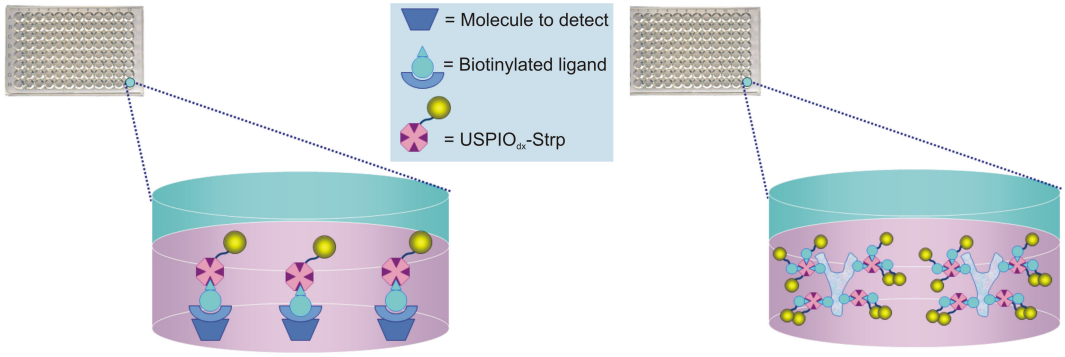

(A)

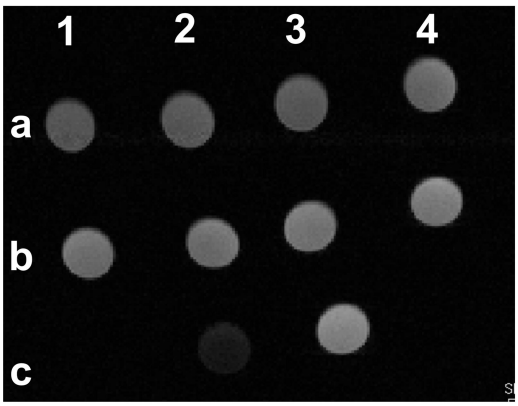

a1:b4 = ranges of [IgG-Bt] incubated with 1 mM USPIO$_{dx}$-Strp and 4 mM USPIO$_{dx}$-Bt
c2 = 0.025 mM USPIO$_{dx}$ in 0.2 M Gly + 1 M Tris-HCl
c3 = 0.2 M Gly + 1 M Tris-HCl

(B)

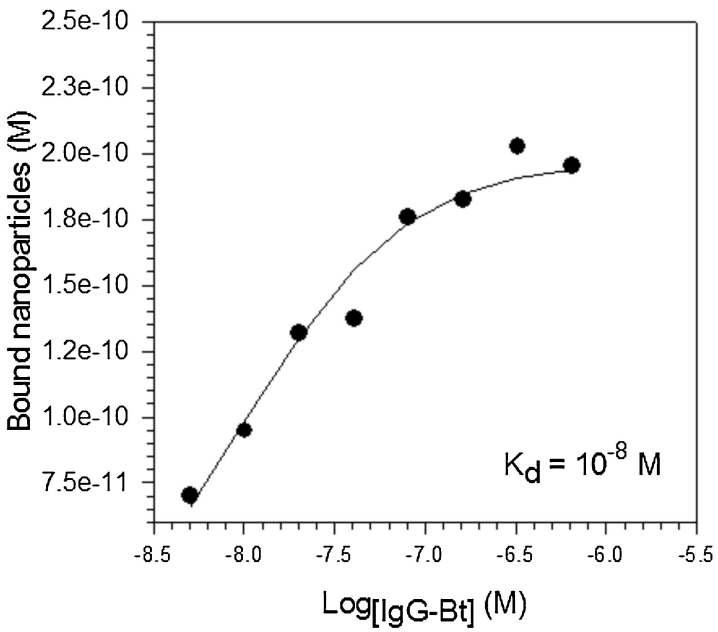

(C)

Figure 2. Interaction of USPIO$_{dx}$-Strp and USPIO$_{dx}$-Bt with IgG-Bt measured by MRI at 4.7 T in a high throughput setting. This setting could be conceived for any biotinylated molecule, but in the present experiment IgG-Bt (0.005–0.64 μM) was immobilized in the wells of a microtiter plate and incubated with constant concentrations of iron oxide nanoparticles (A). T_2 was measured by MRI on the bound nanoparticles dissociated from the surface (B). The R_2^{Norm} was used to estimate the concentration of bound nanoparticles and the K_d of this molecular interaction was calculated (C).

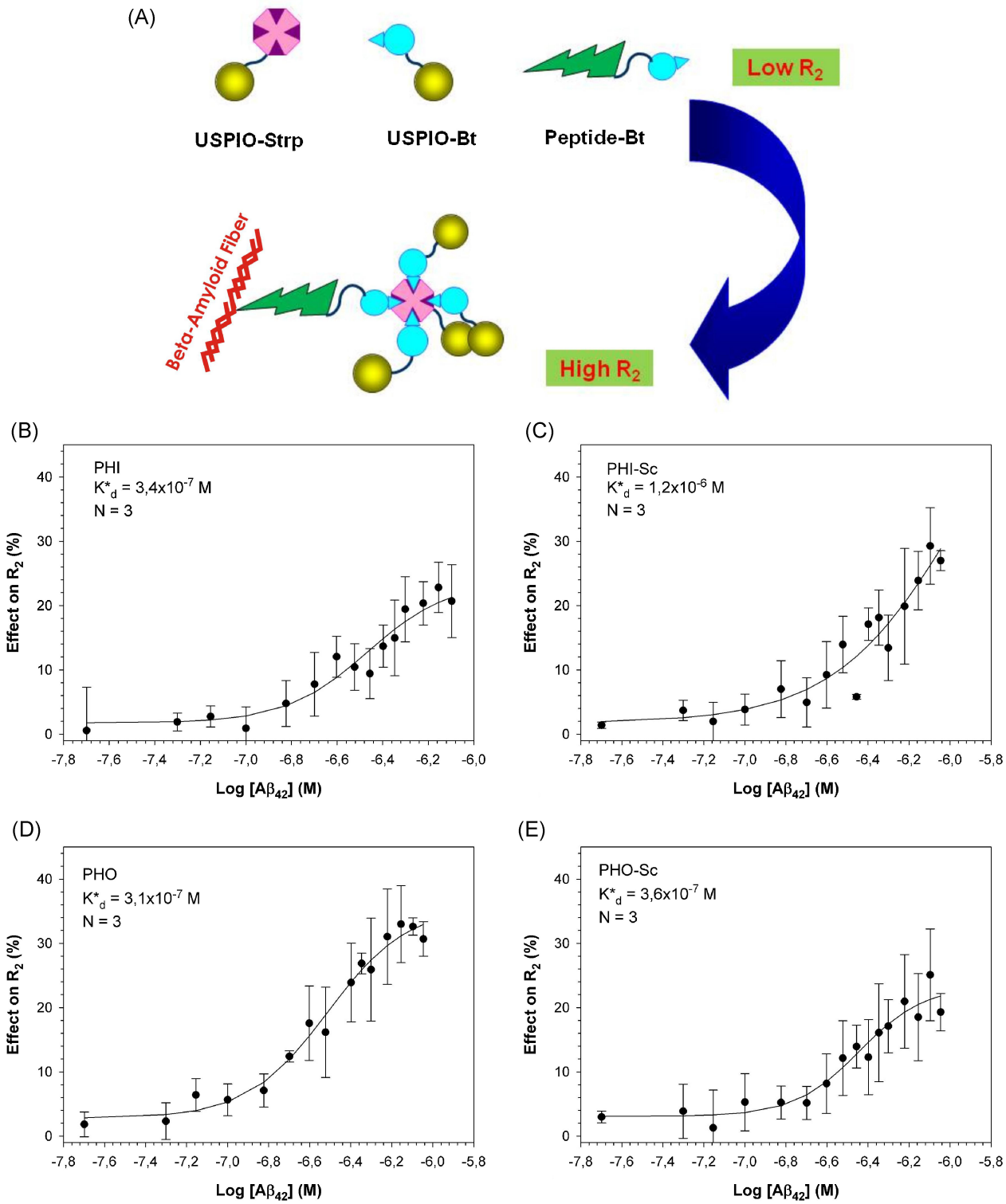

Figure 3. USPIO$_{dx}$-Strp and USPIO$_{dx}$-Bt were used to measure by relaxometry (60 MHz, 37 °C) the molecular interaction between biotinylated cyclic heptapeptides and the beta-amyloid fiber as it is schematically represented in (A). The percentage effect produced on R_2 by this molecular interaction was used to construct the saturation curves of biotinylated peptides (B = PHI, C = PHI-Sc, D = PHO and E = PHO-Sc) against Aβ_{42} and finally to estimate the K^*_d of each of the four peptides.

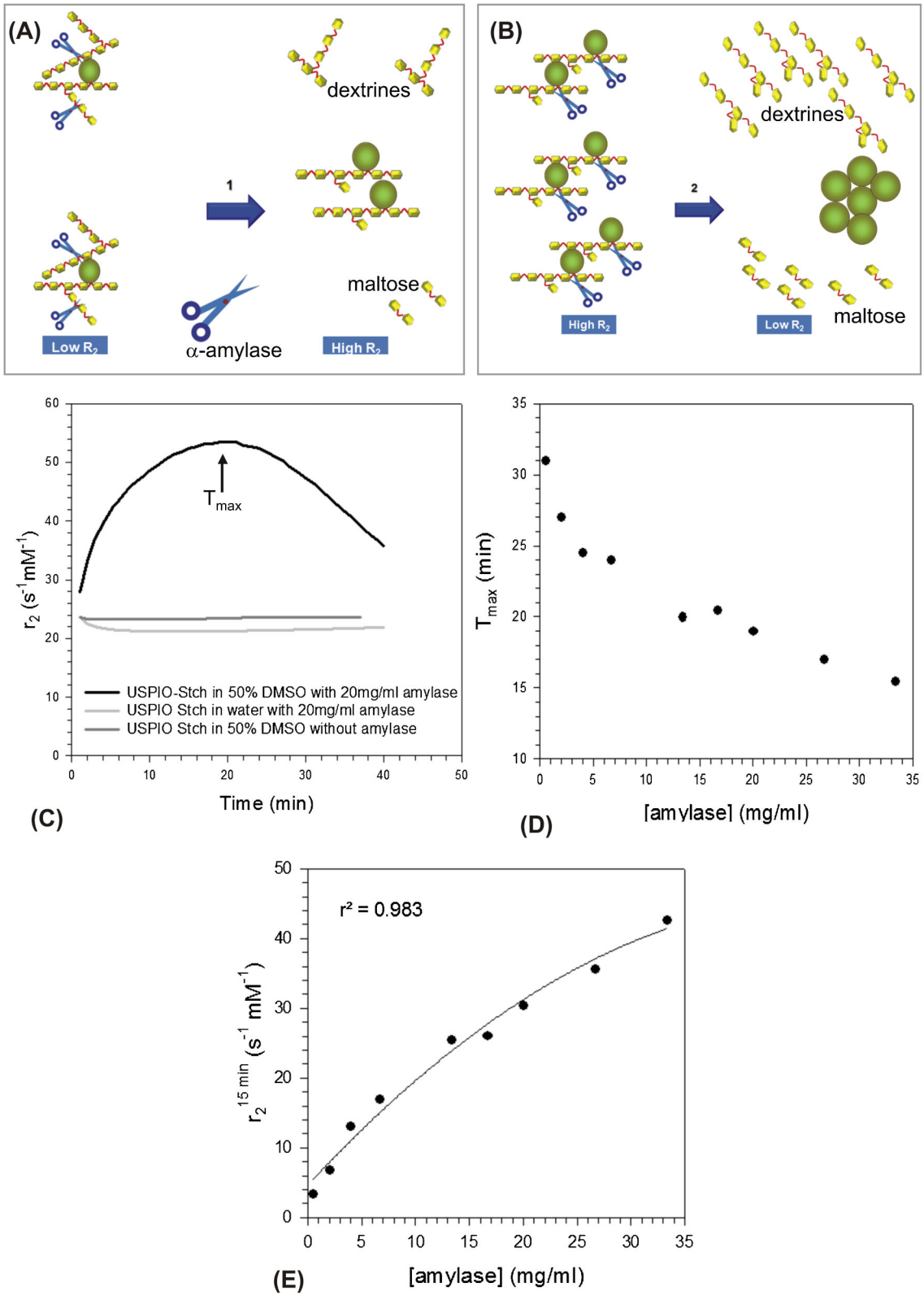

Figure 4. Relaxometric (60 MHz, 37 °C) measurement of amylase activity by using starch-coated USPIO (USPIO-Stch). The schema shows that starch of USPIO-Stch is hydrolyzed by amylase in dextrines and maltose leading in a first stage to an increase of r_2 subsequent to the degradation of the starch matrix (A). After an exhaustive starch hydrolysis, the nanoparticles are released from their coating and precipitate, leading to the decrease of R_2 (B). The r_2 of 1 mM USPIO-Stch solutions stored in 50% DMSO or water and in the presence or in the absence of 20 mg ml^{-1} α-amylase was measured at 60 MHz; when measured in 50% DMSO, the r_2 has a bell-shape time evolution attaining a maximum (T_{max}) after about 20 min of amylase activity (C). The time required to attain the maximum r_2 in a solution of 1 mM USPIO-Stch incubated with various concentrations of α-amylase is shown in (D). The evolution of r_2 measured 15 min after incubation with various concentrations of α-amylase is presented in (E).

2.3. MRI detection of molecular interaction in an ELISA system

A simple ELISA system is exemplified in Figure 2, where interacting molecules could be immobilized on the plastic surface of a microtitration plate in a high-throughput setting and then detected with USPIO derivatives (Fig. 2A) by the MRI measurement of T_2 relaxation times. In our example, IgG-Bt immobilized on the ELISA plate at various concentrations could be detected by MRI (Fig. 2B) subsequent to the interaction with $USPIO_{dx}$-Strp (1 mM) and $USPIO_{dx}$-Bt (4 mM). The bound USPIO derivatives could then be dissociated from the surface, and the T_2 values of the solutions were measured by MRI. The iron concentration could be estimated using a reference sample, and the apparent dissociation constant (K^*_d) was calculated as an example of the type of evaluation that could be obtained by this method (Fig. 2C).

2.4. Measurement of molecular interaction in solution by NMR relaxometry

To assess the molecular interaction in aqueous solution by NMR relaxometry, two $A\beta_{42}$-specific peptides, PHO (hydrophobic) and PHI (hydrophilic), and their scrambled homologs (PHO-Sc and PHI-Sc, respectively) (30) were biotinylated and incubated with various concentrations of their target ($A\beta_{42}$ amyloid peptide). After labeling the bound biomolecules with $USPIO_{dx}$-Strp (10 μM) and $USPIO_{dx}$-Bt (40 μM), the R_2 of the solutions was evaluated by NMR relaxometry (Fig. 3A). The R_2 increased with increasing $A\beta_{42}$ concentration (Fig. 3B–E) for each of the four peptides, which suggests that their binding to $A\beta_{42}$ limits the molecular mobility of the linked USPIO. The highest effect on R_2 (>30%) was observed in the case of PHO (Fig. 3D). The titration curves allowed us to compute the K^*_d of the four peptides, which was in the same range for PHI, PHO and PHO-Sc (3.4×10^{-7}, 3.1×10^{-7} and 3.6×10^{-7} M, respectively) but weaker for PHI-Sc (1.2×10^{-6} M). These K^*_d values are at least two orders of magnitude stronger than those determined by ELISA (in the range of 10^{-5} M for PHI, PHO and PHO-Sc, and 9×10^{-4} M for PHI-Sc) in a previous study (30). Of course, these values are not directly comparable because the methods are different, but a similar tendency between these results could be observed. Indeed, they both showed that the affinity of PHI-Sc is inferior to that of PHI, and that PHO and PHO-Sc have a similar affinity. We have previously observed (30) that values obtained by NMR relaxometry indicate higher affinity constants and we have assumed that polyvalent exposure of peptides (maybe bound to streptavidin in this case) may reproduce the avidity effect of phages or that NMR relaxometry is more sensitive than ELISA.

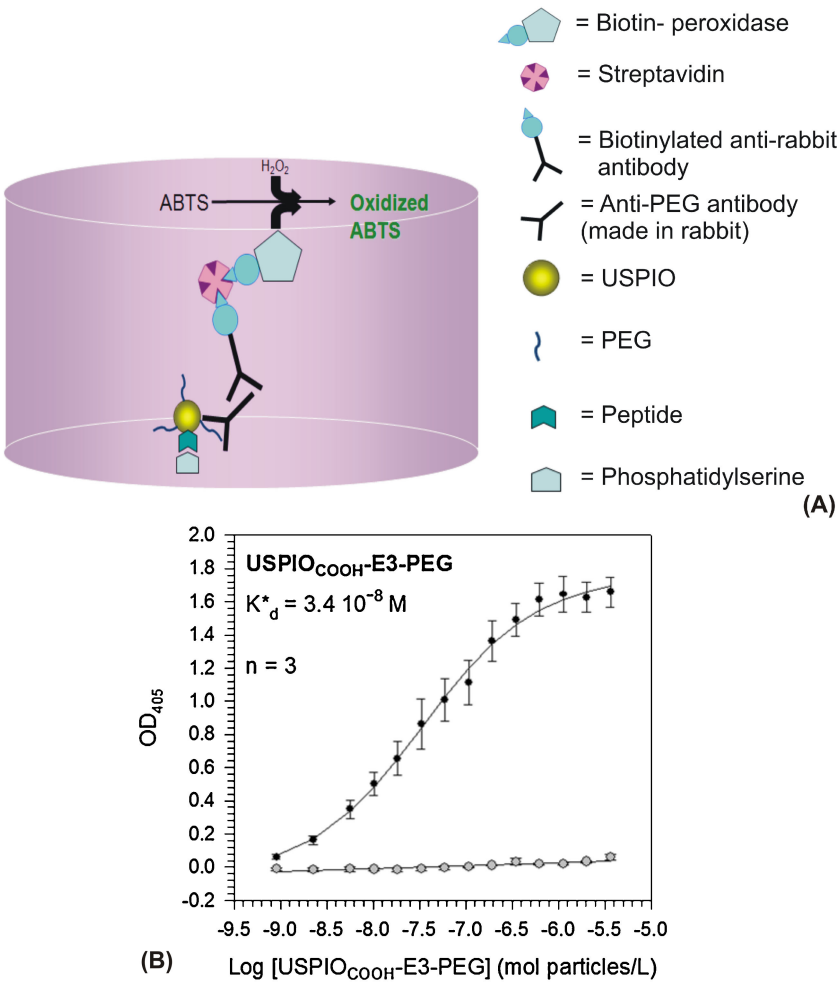

Figure 5. Schematic representation of the experimental setting involving successive antibodies and peroxidase staining reaction for the detection of an apoptosis-targeted USPIO derivative, $USPIO_{COOH}$-E3-PEG (A) and estimation of its K^*_d (B).

2.5. Relaxometric evaluation of amylase activity subsequent to the hydrolysis of USPIO's starch coating

The digestive enzyme α-amylase, classified as a saccharidase, is present in saliva and in the pancreatic juice, where it hydrolyzes the long-chain carbohydrates (e.g. starch) down to maltose and dextrines. This enzyme is also present in blood plasma and in urine, where it is generally measured for the diagnosis of various pathologies, such as the acute and chronic pancreatitis, pancreatic duct obstruction and cystic fibrosis, cancer of the pancreas, diseases of the salivary glands (e.g. mumps, tumors), alcoholism, renal failure, etc.

The present example of application (31,32) aimed at evaluating by relaxometry the amylase enzymatic activity using a starch coated USPIO (USPIO-Stch) as a substrate (Fig. 4A and B). During the hydrolysis of the starch coating of USPIO (1 mM) subsequent to amylase (20 mg ml^{-1}) activity (Fig. 4A), the transverse relaxivity (r_2) followed a bell-shape curve (Fig. 4C). The time required to attain the maximum r_2 was defined as T_{max}. No T_{max} could be observed in the absence of amylase or for the same nanoparticles not conserved in DMSO. In the case of USPIO-Stch conserved in DMSO, T_{max} depended on the amylase concentration (Fig. 4D). Aiming to simplify the protocol, only one measurement can be performed after an optimal time of incubation, time that must be situated in the same range of the r_2 evolution for all the test samples. For instance, a measurement after 15 min of incubation at 37 °C allowed evaluating r_2 before T_{max}, in the domain of r_2 augmentation, for all the assessed amylase concentrations (Fig. 4E). The results were reproducible in time, the r_2/r_1 being constant until 10 days of assessment in the same conditions (data not shown).

2.6. In vitro detection of functionalized USPIO by ELISA and MRI

2.6.1. *ELISA applications of functionalized USPIO derivatives*

Functionalized USPIO have been detected with antibodies in a classical ELISA experiment. In the example shown in Fig. 5, $USPIO_{COOH}$ were functionalized with a peptide (E3) specific to apoptotic cells (27,33) and rendered furtive by grafting PEG_{750} moieties ($USPIO_{COOH}$-E3-PEG). The nanoparticles bound to phosphatidylserine (PS) were detected with an anti-PEG antibody, which was then identified by a biotinylated secondary antibody, followed by streptavidin and peroxidase-biotin (Fig. 5A). The K^*_d of $USPIO_{COOH}$-E3-PEG estimated by this method was 3.4×10^{-8} M (Fig. 5B), which is about 10 times stronger than that of the non-conjugated peptide (3.34×10^{-7} M) (27), probably suggesting a polyvalent mechanism of PS binding.

Functionalized USPIO derivatives could replace antibodies in ELISA protocols, the Perls' staining reaction rendering possible the detection of USPIO interaction with specific molecules immobilized on microtiter plates. This application was validated using $USPIO_{dx}$-R826 incubated in a range of concentrations with PS immobilized on an ELISA plate. The nanoparticles bound to the target were digested in acidic conditions and the iron could be quantified by Perls' staining (34). The K^*_d for PS binding of $USPIO_{dx}$-R826 could be estimated (Fig. 6A) after converting the iron concentration into moles of nanoparticles. $USPIO_{dx}$-R826 did

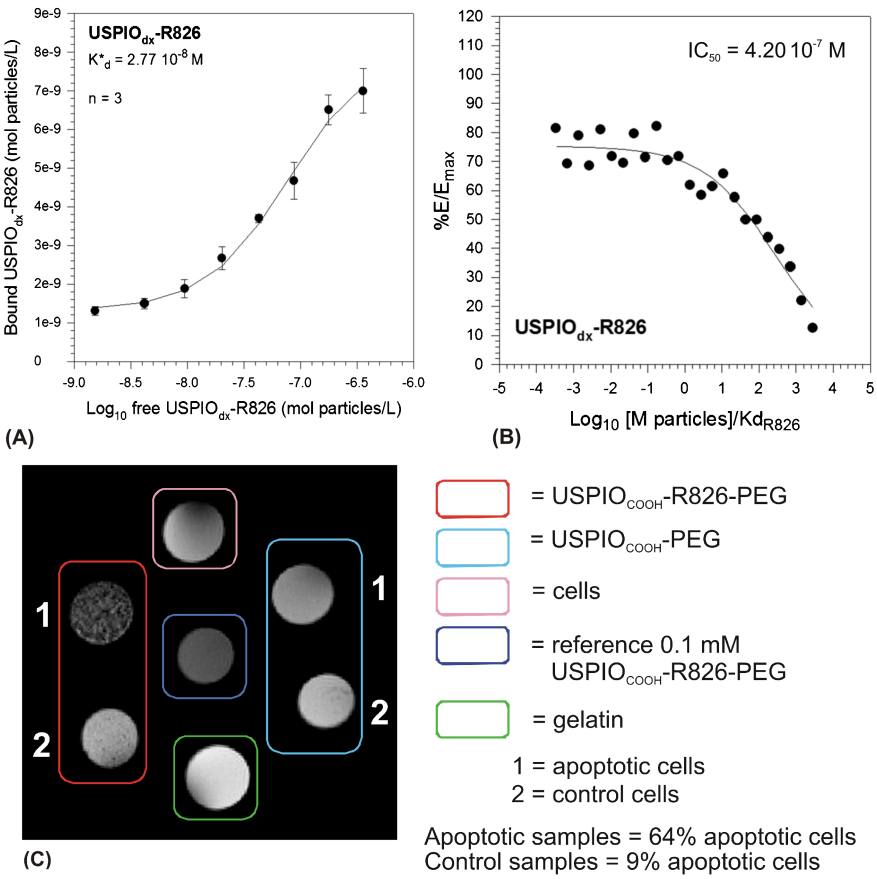

Figure 6. *In vitro* detection of USPIO derivatives vectorized to apoptotic cells ($USPIO_{dx}$-R826 and $USPIO_{COOH}$-R826-PEG) by ELISA (A, B) and MRI (C).

not show any non-specific binding to BSA-coated ELISA plate (data not shown).

In another experimental setting, the IC_{50} was estimated for $USPIO_{dx}$-R826 which was submitted to a competition with annexin V (AnnV) (Fig. 6B). During this experiment, the target (PS) is pre-incubated with various concentrations of $USPIO_{dx}$-R826 and is subsequently exposed to the competitor (AnnV), which is added at a concentration equal to its K_d. In this experiment, AnnV is biotinylated (AnnV-Bt) and detected with peroxidase-conjugated streptavidin. The calculated IC_{50} of $USPIO_{dx}$-R826 (4.20×10^{-7} M) is about 30 times weaker than that of the non-conjugated peptide (1.48×10^{-8} M) (28).

2.6.2. *MRI visualization of cells*

The *in vitro* visualization of cells by MRI subsequent to being labeled with specifically targeted USPIO derivatives is a simple and rapid approach that could be used, for instance, to validate the cancer diagnosis on biopsy specimens. The method is sensitive, requires minimal sample preparation and employs USPIO derivatives functionalized with cost-effective peptides. To evaluate this approach, $USPIO_{COOH}$ functionalized with a peptide specific to apoptotic cells (28) ($USPIO_{COOH}$-R826-PEG) was incubated with apoptotic and control Jurkat T lymphocytes, and visualized by MRI (Fig. 6C). The MR image indicates that $USPIO_{COOH}$-R826-PEG produced an important contrast between apoptotic and control cells, which was not possible with non-functionalized $USPIO_{COOH}$. Subsequently, $USPIO_{COOH}$-R826-PEG was used to develop other *in vitro* protocols for biomedical applications as discussed below.

2.7. Detection of specific biomolecules by histochemistry

Thanks to their iron core, the functionalized nanoparticles bound to specific biomolecules expressed by the cells in histological samples can be easily detected by Perls' Prussian blue staining,

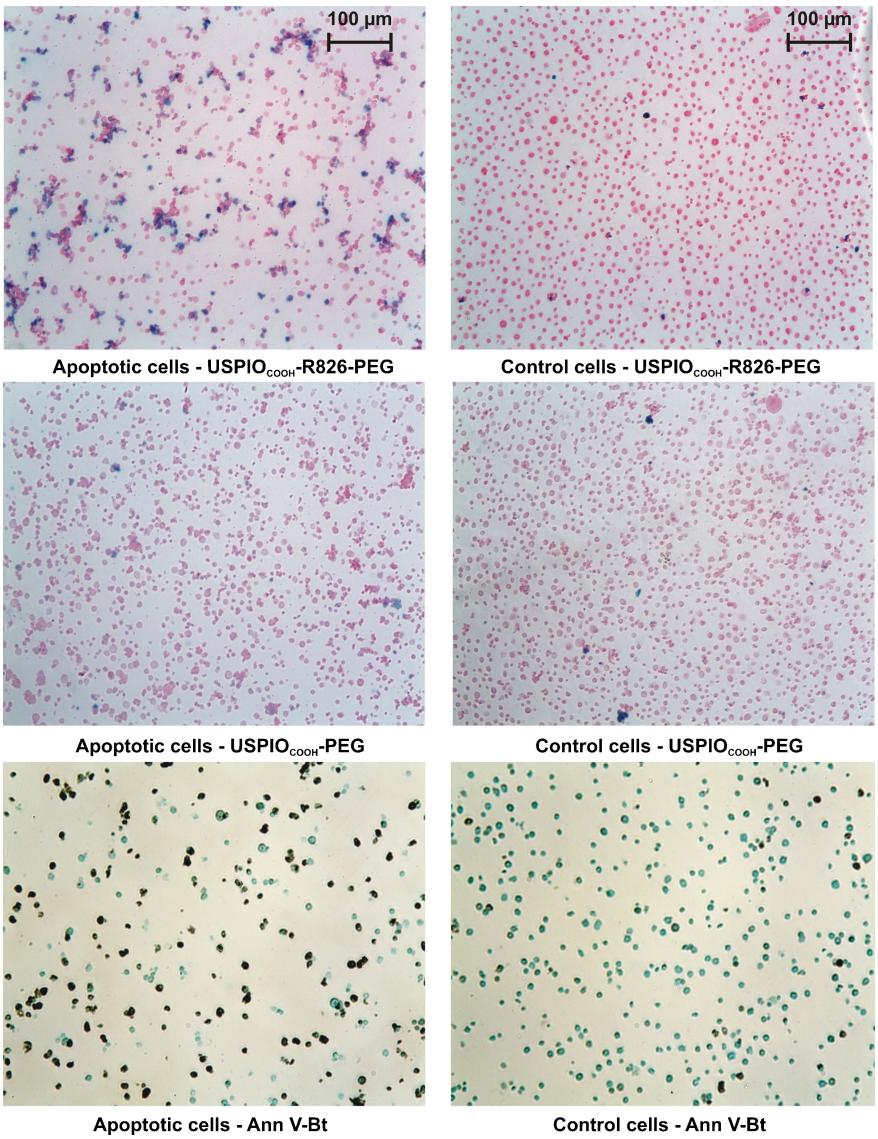

Figure 7. Detection of apoptotic cells by cytochemistry. The cells were incubated with $USPIO_{COOH}$-R826-PEG or $USPIO_{COOH}$ and the iron was stained by the Perls' Prussian Blue method, followed by counterstaining with eosin. The staining of apoptotic cells was confirmed with AnnV-Bt, the brown staining being developed with DAB followed by counterstaining with Luxol fast blue.

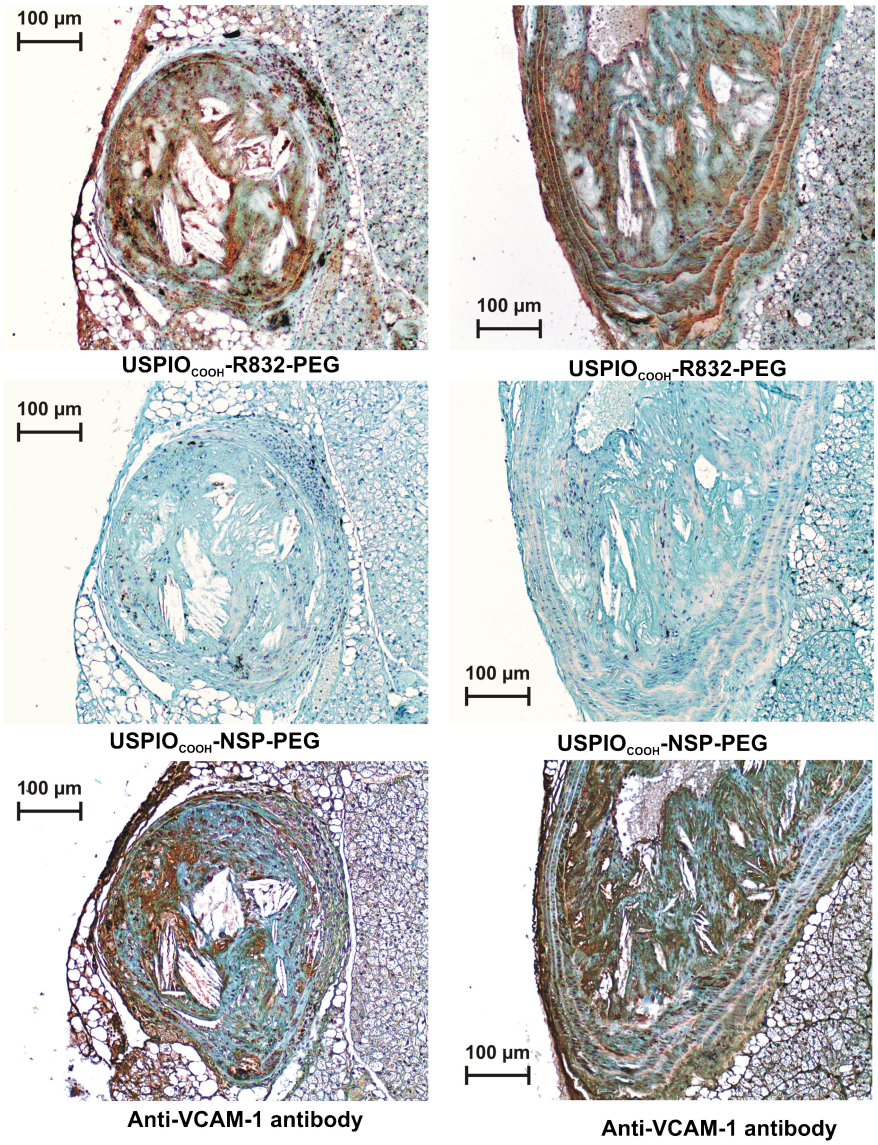

Figure 8. Histochemistry of VCAM-1 expression in atherosclerotic plaque of ApoE$^{-/-}$ mice. The aorta was incubated with USPIO$_{COOH}$-R832-PEG or with USPIO$_{COOH}$-NSP-PEG and the iron was stained by the Perls'-DAB method. The staining of VCAM-1 was confirmed with anti-VCAM-1 antibody, the brown staining being developed with DAB followed by counterstaining with Luxol fast blue.

substituting thus the need for antibodies. To assess this possibility, we have used two types of functionalized USPIO$_{COOH}$ nanoparticles: specific to apoptotic cells (USPIO$_{COOH}$-R826-PEG) (28) or to VCAM-1 over-expressed in inflammatory pathologies (USPIO$_{COOH}$-R832-PEG) (29).

The first experiment was carried out with apoptotic Jurkat cells which were stained with USPIO$_{COOH}$-R826-PEG and compared with the staining produced by AnnV-Bt (Fig. 7). The two compounds specifically labeled the dead cells (treated with camptothecin), while the control cells remained unstained; the few cells that were stained in the control sample could conceivably be dead cells present in this sample.

In the second experiment, VCAM-1 expressed by atherosclerotic plaque of ApoE$^{-/-}$ mice was stained with either USPIO$_{COOH}$-R832-PEG or with anti-VCAM-1 antibody (Fig. 8). The two compounds showed a similar staining pattern, while the control nanoparticles conjugated to a non-specific peptide (USPIO$_{COOH}$-NSP-PEG) did not produce any significant staining.

3. Conclusions

The *in vitro* biomedical applications proposed by the present work for functionalized magnetic nanosensors sustain the rapid and simple detection of a diversity of biomolecules with relevance for medicine. The protocols involving such devices can be applied to minimally prepared biological samples (e.g. whole blood, blood plasma or serum, cell suspensions, biopsies, histological preparations, etc.), and often do not need complicated systems of signal amplification. The detection of bound iron oxide can be carried out in solution or on microarray immobilized biomolecules, cells or tissues, the measurement being possible by NMR equipment or by using chemically staining reactions. In the case of NMR equipment, the sample turbidity does not significantly interfere with the sensitivity of the measurement done in solution, but the relaxation rate could follow an ascending or a descending slope depending on the size of the nanoassembly that is formed subsequent to molecular

interaction, especially in the case of enzymes. In this situation, a certain domain of the relaxation rate evolution should be selected for the evaluation of a range of the substrate or target concentrations. The direct labeling of the binding molecule with magnetic nanosensors allows the real-time and real-state estimation of the binding kinetics, while the results can be converted into number of molecules bound to the target which is sometimes essential for an accurate decision in diagnostic or pharmacological screening methodology. The MRI equipment allows even the concomitant analysis of a large number of microtiter plates, as opposed to the classical ELISA plate readers, assisting thus in the high-throughput screening of new drug targets and therapeutic molecules. The key for the routine implementation of such an application is however strongly conditioned by the development of portable bench-top NMR screening equipment. The chemically staining reactions, such as Perls' iron staining, is another methodology that could be applied both in ELISA or in histological settings, while the use of SPION labeled compounds could be more cost-effective as compared to the battery of expensive ELISA-dedicated compounds. The use of peptides instead of antibodies to functionalize SPION, as in the present work, could furthermore contribute to cost reductions in diagnosis and in patient care. The outstanding development of biosynthetic technologies nowadays (35,36) is susceptible to render the expense of peptide synthesis more profitable, with production yields that are much improved over the classical chemical routes. The biosynthetic technologies were even exploited in the synthesis of particulate inorganic material, which is produced by various mono-cellular organisms, the magnetotactic bacteria being able to synthesize magnetite (37). However, the chemical synthesis of SPION is already very economic, and the functionalized material could be detected by ELISA subsequent to iron staining at a concentration of 2.7×10^{-9} M particles (as shown in Fig. 6) with no need for signal amplification produced by supplementary antibodies and color revelation mixtures. The same is possible by histochemistry, the detected concentration being, in our experimental conditions, of 9×10^{-8} M particles (as shown in Fig. 8). This reduces the cost of the test by at least a factor of two or three if we take into account the number of antibodies that are not included in the detection protocol. The sensitivity of the test could be improved by increasing the size of SPION and hence the iron payload per particle. The detection sensitivity is also improved when the molecular interaction is measured in a relaxometric setup (as shown in application 4, Fig. 3), which also allows the exclusion of serial interacting antibodies that are often responsible for the expensiveness of the diagnosis tests. However, the standardization of SPION concentrations for Perls' staining or MRI protocols is undemanding, but the relaxometric methods seem to be more challenging for standardization since the T_2 can be either prolonged or decreased as a function of the size of the supramolecular aggregate. Various SPION preparations are commercially available worldwide, and their functionalization is versatile (7) and is facilitated by ready to use conjugation kits. Their applications are not limited to the laboratory of clinical diagnosis, but any biomedical research environment can take profit of this new technology. Functionalized SPION preparations could be conceived in standardized kit formulations and designed to identify or quantify any type of biomolecule with interest for medicine. In these conditions, the test is simplified to a few easy steps, which could tolerate the automation of the analysis process.

4. Experimental procedures

4.1. Preparation of functionalized USPIO derivatives

4.1.1. Conjugation of streptavidin, biotin or peptides to $USPIO_{dx}$

The dextran-coating of $USPIO_{dx}$ particles was crosslinked with epichlorhydrin and aminated to allow for the grafting (21,38) of Strp, Bt, or peptides. Five milliliters of USPIO (100 mg of Fe, dextran coated maghemite particles with a hydrodynamic size of 22 nm) were diluted in 25 ml of water and treated with 20 ml of NaOH 5N and 10 ml of epichlorhydrin. The mixture was stirred for 24 h at 40 °C in the dark and then dialyzed (cut-off of the membrane, 12 000–14 000; Spectra/Por, VWR, Leuven, Belgium) in a 5 mM sodium citrate buffer (pH = 8). A solution of Strp (5 mg, Sigma-Aldrich, Bornem, Belgium) or Bt (5 mg, Sigma-Aldrich) in 2 ml of water was added to the USPIO–epichlorhydrin suspension (90 μmol of Fe). For grafting the peptides, a volume of 0.2 ml USPIO–epichlorhydrin (250 mM Fe) was added to 7 μmol of peptide (R826) in aqueous solution. The mixture was stirred at room temperature overnight and was exhaustively dialyzed to remove the free non-conjugated molecules.

4.1.2. Conjugation of peptides to $USPIO_{COOH}$

The peptides (E3, R826 and R832, NSP) (27–29) were purchased as 8-amino-3,6-dioxaoctanoyl derivatives (NeoMPS, Strasbourg, France) and with Lys protected by trifluoroacetic acid. They were conjugated to $USPIO_{COOH}$ through their amino-terminal groups as previously described (39). PEG-NH_2 $M_w \approx 750$ g mol^{-1} [O-(2-aminoethyl)-O′-methylpolyethyleneglycol; Sigma-Aldrich] was finally conjugated to the free carboxyl groups exposed by the bisphosphonate coating of the particles. Peptides were then unprotected with a solution of 1 M NaOH, and the pH was finally adjusted to 7.5. To remove the free non-conjugated molecules, the solution was exhaustively dialyzed.

4.1.3. Synthesis of starch-coated USPIO (USPIO-Stch)

To prepare starch-coated USPIO, 0.53 g $FeCl_2 \cdot 4\,H_2O$, 0.17 g $FeCl_3 \cdot 6\,H_2O$ (Fe^{2+}:Fe^{3+} ratio of 4:1) and 2.5 g of potato starch pretreated with glycerol at 190 °C (Sigma-Aldrich) were solubilized in 250 ml of 0.031% HCl (nitrogen gas bubbled into the solution to prevent Fe^{2+} oxidation) and mixed with 250 ml of 0.82% NH_3 after heating the solutions at 70 °C in a water bath. The two solutions were then progressively mixed in a reactor heated to 80 °C and nitrogen gas was subsequently bubbled in for 15 min.

4.1.4. Physico-chemical characterization

The mean diameter of the coated nanoparticles was of 50 nm for USPIO-Stch and of about 30 nm for all the other USPIO derivatives. Hydrodynamic size measurements were carried out by photon correlation spectroscopy (PCS) on a Brookhaven system BI-160 (New York, USA) equipped with a He–Ne laser ($\lambda = 633$ nm, 35 mW), a goniometer and a correlator BI-9000AT-BC or on a Malvern system (Zêtasizer Nanoseries ZEN 3600). Iron concentration was determined by relaxometry at 20 MHz (Bruker Minispec, Bruker, Karlsruhe, Germany) and 37 °C after mineralization in acidic conditions (0.6 ml HNO_3 and 0.3 ml H_2O_2) by microwaves (Milestone MSL-1200, Sorisole, Italy). Protein or peptide concentration in the suspension of USPIO derivatives was determined by Bio-Rad protein assay (Bio-Rad Laboratories SA-NV, Nazareth, Belgium), and it was calculated to

Table 1. Proton relaxivities (r_1 and r_2) of USPIO derivatives as measured at 60 MHz and 37 °C

USPIO derivative	r_1 (s^{-1} mM^{-1})	r_2 (s^{-1} mM^{-1})	r_2/r_1
$USPIO_{dx}$	10.1	63.1	6.25
$USPIO_{dx}$-Strp	11.6	91.2	7.86
$USPIO_{dx}$-Bt	10.2	77.9	7.64
$USPIO_{dx}$-R824	14.6	96.1	6.58
$USPIO_{dx}$-R825	14.4	95.9	6.66
$USPIO_{dx}$-R826	14.9	93.1	6.25
$USPIO_{COOH}$-PEG	17.0	74.3	4.37
$USPIO_{COOH}$-R826-PEG	15.7	88.5	5.64
$USPIO_{COOH}$-E3-PEG	15.5	70.4	4.54
$USPIO_{COOH}$-R832-PEG	14.6	82.3	5.64
$USPIO_{COOH}$-NSP-PEG	16.9	85.7	5.07
USPIO-Stch (in 50% DMSO)	2.9	23.9	8.3

be of about two protein molecules per particle in the case of $USPIO_{dx}$-Strp, and of about three to five molecules per particle in the case of peptide-functionalized USPIO derivatives; one USPIO nanoparticle was assumed to contain an average of 11 000 iron atoms (21). Their proton transverse relaxivities (r_2) were measured at 60 MHz and 37 °C on a Bruker Minispec mq60 (Table 1).

4.2. Interaction of $USPIO_{dx}$-Strp and $USPIO_{dx}$-Bt with IgG-Bt measured by relaxometry and MRI

IgGs from human serum (Sigma-Aldrich) were biotinylated (IgG-Bt) by the reaction with an excess of biotin in the presence of EDC [1-ethyl-3-(3-dimethylaminopropyl) carbodiimide], the excess of biotin was eliminated by dialysis, and the IgG-Bt were finally solubilized in a physiologic solution at a concentration of 4 μM. Various dilutions (ranging between 0.01 and 1.8 μM) of the stock solution in PBS were incubated at 37 °C with 10 μM of $USPIO_{dx}$-Strp and 40 μM of $USPIO_{dx}$-Bt. T_2 relaxation times of USPIO solutions (independently or combined) were measured at 60 MHz on a Bruker Minispec mq60 before and after the addition of IgG-Bt. The time-dependence of the molecular interaction was followed-up until 63 min of incubation. The normalized relaxation rate (R_2^{Norm}) was calculated and defined as $R_2^{obs} - R_2^{Ref}$, where R_2^{obs} is the observed R_2 of the samples whereas R_2^{Ref} is the R_2 of the reference solution which was prepared similarly to the test samples but by substituting IgG-Bt with an equivalent volume of PBS.

For MRI, IgG-Bt was immobilized at various concentrations (0.005–0.64 μM) on protein A-coated ELISA plates (Reacti-Bind™ plates, Pierce, Perbio Science, Erembodegem-AALST, Belgium) and incubated at 37 °C with 1 mM $USPIO_{dx}$-Strp (2h) and 4 mM $USPIO_{dx}$-Bt (30 min). After each of the incubations, the unbound ligands were rinsed three times with 200 μl of PBS. Finally, the bound ligands were re-suspended with 100 μl of 0.2 M glycine, pH 2.2, neutralized with 15 μl of 1 M Tris–HCl, pH 9.1, and analyzed by MRI at 4.7 T on a Bruker Avance-200 imaging system (Bruker, Ettlingen, Germany) using a spin-echo imaging sequence ($TR/TE = 3000/20$ ms, 40 echoes, FOV = 5 cm, slice thickness = 1.6 mm, matrix = 256 × 256). The T_2 values were measured on images and the Fe concentration was estimated by using a reference sample of 25 μM $USPIO_{dx}$ prepared in a solution of glycine/Tris–HCl. The dissociation constant of this molecular interaction was then calculated (21).

4.3. Interaction of $USPIO_{dx}$-Strp and $USPIO_{dx}$-Bt with Aβ_{42}-specific biotinylated peptides measured by relaxometry

Peptides (30) were purchased as 8-amino-3,6-dioxaoctanoyl derivatives and biotinylated (NeoMPS, Strasbourg, France). Each biotinylated peptide was incubated (60 min at 37 °C) at 10^{-6} M in PBS with a range of concentrations (10^{-8}–10^{-6} M) of $A\beta_{42}$ (Bachem AG, Bubendorf, Switzerland). USPIO-Stp (10 μM) and USPIO-Bt (40 μM) were then added and the mixture was incubated for 3 min at 37 °C. T_2 relaxation times were measured on a Bruker mq60 Minispec. The R_2^{Ref} was obtained as described above by substituting $A\beta_{42}$ with an equivalent volume of PBS. The percentage effect (% effect) of $A\beta_{42}$ on R_2 was computed using the following equation:

$$\text{Effect} = \frac{R_2{}^{A\beta} - R_2{}^{Ref}}{R_2{}^{Ref}} * 100$$

where $R_2^{\beta A}$ is the transverse relaxation rate of samples.

4.4. Measurement of the T-cell receptor (CD3) expression by relaxometry

Jurkat T lymphocytes (2×10^6 ml^{-1}) cultured as previously described (21) were first blocked with 100 μg ml^{-1} of streptavidin (5 min, 37 °C), and then with 400 μg ml^{-1} of biotin (5 min, 37 °C). The cells (2×10^6 to 0.15×10^6) were then incubated (1 h, room temperature) with mouse anti-human CD3 biotin-conjugated monoclonal antibody (Chemicon International, Biognost, Heule, Belgium) diluted to 1:10 in the culture medium. The antibody bound to the cells was detected by incubation with 10 μM of $USPIO_{dx}$-Strp (5 min, room temperature) and then with 40 μM of $USPIO_{dx}$-Bt (5 min, room temperature). The cells were rinsed with PBS after each of the incubations and were finally re-suspended in PBS. The T_2 was measured on a Bruker mq60 Minispec and the R_2^{Norm} was calculated as described above, with R_2^{Ref} being the R_2 of cells not incubated with anti-CD3 antibody but incubated with USPIO derivatives.

4.5. Relaxometric measurement of amylase activity

USPIO-Stch was conserved in 50% DMSO, which limits the starch retrogradation and optimizes the amylase activity. For the measurement of the α-amylases (from *Bacillus subtilis*,

~380 U mg^{-1}, Sigma Aldrich) effect on R_2, USPIO-Stch (at a concentration of 1 mM Fe and containing 1.5 g of starch l^{-1}) was incubated (15 min, 37 °C) with a range of amylase concentrations (0.5–33 mg ml^{-1}) diluted in 0.1 M K_2HPO_4, pH 6.7. The T_2 relaxation time was measured on a Bruker mq60 Minispec and R_2^{Norm} was calculated by subtracting the r_2 of USPIO-Stch from R_2^{obs}.

4.6. ELISA and MRI detection of USPIO vectorized to apoptotic cells

4.6.1. ELISA: estimation of the K$^*_d$ *of USPIO$_{COOH}$-E3-PEG by peroxidase staining reaction*

PS was immobilized on microtiter plates (100 μg ml^{-1}, 20 μg per well) and the wells were then blocked with Protein-Free Blocking Buffer (PFBB, Perbio Science, Erembodegem, Belgium). The wells were rinsed three times with Ca^{2+} buffer–0.05% Tween-20 (28), and a range of CA concentrations (40–0.01 mM Fe) were prepared in Ca^{2+} buffer completed with 0.05% Tween-20 and 0.5% BSA and incubated (2h, 37 °C) with PS-coated wells. The wells were subsequently washed as described above and the CA bound to PS was detected (1h, room temperature) with 2 μg ml^{-1} of rabbit anti-PEG monoclonal antibody (Epitomics/Bio-Connect BV, TE Huissen, The Netherlands) diluted in Ca^{2+} buffer completed with 0.05% Tween-20 and 0.5% BSA. The primary antibody was subsequently detected with 3 μg ml^{-1} of biotinylated goat anti-rabbit IgG (Vector Labconsult, Brussels, Belgium) and with Vectastain ABC kit (Vector Labconsult). The peroxidase staining reaction was performed as previously described (28).

4.6.2. ELISA: estimation of the K$^*_d$ *of USPIO$_{dx}$-R826 by Perls' staining*

The affinity for PS of USPIO$_{dx}$-R826 was determined by ELISA, by measuring the iron concentration with Perls' Prussian Blue staining reaction (34). The target (PS) was immobilized on microtiter plates as previously described (28) at a concentration of 120 μg ml^{-1} (24 μg per well) and the wells were then blocked (2h, 4 °C) with 0.25 ml per well of the blocking buffer (0.1 M $NaHCO_3$, 0.02% NaN_3, 1% BSA). After washing the wells three times with Ca^{2+} buffer completed with 0.05% Tween-20, two-fold serial dilutions of the CA (4–0.03 mM Fe; 4 mM iron corresponds to 3.63×10^{-7} M particles by assuming ~11 000 iron atoms per particle) were prepared in Ca^{2+} buffer. The PS coated wells were then incubated (2h, 37 °C) with 0.2 ml per well of the CA. The wells were subsequently washed as described above and the CA bound to PS was digested (48 h, 37 °C) with 0.1 ml of 5N HCl. The iron concentration was determined with Prussian Blue, Perls' reagent (Riedel-de Haën, Seelze, Germany; 5% potassium ferrocyanide in distilled water, 0.1 ml per sample, incubation 15–30 min at room temperature, measurement of OD_{630}). To estimate the apparent dissociation constant (K^*_d) of the PS-targeted CA, the iron concentration was converted into moles of particles per liter.

4.6.3. ELISA: estimation of the IC$_{50}$ of USPIO$_{dx}$-R826 by peroxidase staining reaction

PS was immobilized on microtiter plates (100 μg ml^{-1}, 20 μg per well) and the wells were then blocked with 0.25 ml per well of the blocking buffer as described above. After washing the wells three times with Ca^{2+} buffer–0.05% Tween-20, two-fold serial dilutions of USPIO$_{dx}$-R826 were incubated with the PS-coated wells. The USPIO$_{dx}$-R826 concentrations (4.22×10^{-7} M to 5.03×10^{-14} mol of particles l^{-1}) used in this experiment were based on the K^*_d value estimated for the corresponding phage clones (28). After 30 min of incubation at 37 °C, the competitor AnnV–Bt (Sigma-Aldrich) was added at a constant concentration equal to its K_d for PS (5×10^{-10} M). In separate wells, Ann V–Bt was incubated in the absence of USPIO$_{dx}$-R826 to evaluate the uninhibited binding. The incubation at 37 °C was continued for 1h 30 min, and then the wells were washed as described above. AnnV–Bt bound to the target was detected with HRP-conjugated streptavidin (Sigma-Aldrich; 1 h, room temperature). The peroxidase staining reaction was performed with 200 μl per well of ABTS [2,2́-azino-bis(3-ethylbenz-thiazoline-6-sulfonic acid), diamonium salt (Sigma-Aldrich), 22 mg in 100 ml of 50 mM sodium citrate, pH 4.0] completed with 0.05% H_2O_2. The OD_{405} was measured with a Stat Fax-2100 microplate reader (Awareness Technology Inc., Fisher Bioblock Scientific, Tournai, Belgium).

4.6.4. MRI of apoptotic cells

Apoptosis was induced on Jurkat cells with 2 μM camptothecin (MP Biomedicals, Brussels, Belgium) (28,33). Twenty-four hours later, apoptotic and control cells were re-suspended in fresh culture medium at a concentration of 2x10^6 cells ml^{-1} (4 ml per sample) and incubated with CAs (USPIO$_{COOH}$-R826-PEG or USPIO$_{COOH}$-PEG) at a concentration of 2 mM Fe. After 2 h of incubation at 37 °C, the cells were rinsed three times with Ca^{2+} buffer (2.5 mM $CaCl_2$, 150 mM NaCl, 10 mM Hepes, pH 7.4). The final pellet obtained after centrifugation was re-suspended (8×10^6 cells per sample) in 0.2 ml of 2% gelatin prepared in PBS and transferred into 0.2 ml PCR tubes. The samples were analyzed by MRI using a T_2-weighted spin-echo sequence (Bruker Avance-200, 4.7 T, $TR/TE = 3000/60$ ms, matrix $= 256 \times 256$, FOV = 3.5 cm, slice thickness = 1.5 mm, two averages).

4.7. Histochemistry

4.7.1. Detection of apoptotic cells

Apoptosis was induced on Jurkat cells with 2 μM camptothecin. Twenty-four hours later, apoptotic and control cells were re-suspended in fresh culture medium at a concentration of 2×10^6 cells ml^{-1}. Apoptotic cells were detected either with USPIO$_{COOH}$-R826-PEG, which was stained with Perls' reagent, or with AnnV-Bt, which was stained by peroxidase staining reaction.

4.7.1.1 Perls' staining: The cells were incubated (2 h, room temperature) with USPIO$_{COOH}$-R826-PEG (3 mM Fe). USPIO$_{COOH}$-PEG was used as a negative control compound. After rinsing three times (8000 rpm, 15 min) with Ca^{2+} buffer, the cells were immobilized on 0.01% poly-L-Lys (Invitrogen, Merelbeke, Belgium) coated cover-slips and fixed (15 min, room temperature) with 2 ml of 4% buffered paraformaldehyde. The nanoparticles bound to the cells were stained (15 min, room temperature) with Perls's working solution (mixing equal volumes of 2% potassium ferrocyanide and 2% HCl). Cells were counterstained with 0.5% eosin (30 s), rinsed in tap water and in distilled water, and finally mounted in a permanent medium.

4.7.1.2 Immunocytochemistry: Endogenous peroxidases were blocked with 0.06% H_2O_2, while endogenous biotin was blocked with a blocking kit (Invitrogen). The cells were subsequently immunostained (28) with 5 μl ml^{-1} of AnnV-Bt (Fisher Bioblock Scientific) diluted in culture medium (30 min, room temperature). The cells labeled with AnnV-Bt were immobilized on cover-slips and fixed as described above. After incubation with

streptavidin-linked peroxydase complexes (ABC kit, DakoCytomation SAS, Trappes, France), the samples were incubated 5 min with 50 mM Tris–HCl, pH 7.4, and then stained with 0.05% 3,3′-diaminobenzidine (DAB) completed with 0.02% H_2O_2 in PBS. Cells were counterstained with Luxol fast blue and mounted in a permanent medium.

4.7.2. *Detection of VCAM-1 expression*

Aorta samples collected from ApoE$^{-/-}$ mice (29) were fixed by immersion in Duboscq–Brazil solution, embedded in paraffin, and 5 μm thick sections were finally cut. VCAM-1 expression was detected either with USPIO$_{COOH}$-R832-PEG by Perls's-DAB staining or with a dedicated anti-VCAM-1 antibody by immunohistochemistry.

4.7.2.1 Perls'-DAB staining: After rehydration of histological samples, endogenous peroxidases were blocked for 10 min with 1% H_2O_2 in PBS. VCAM-1 expression was detected by overnight incubation with USPIO$_{COOH}$-R832-PEG (1 mM Fe) diluted in TBS (50 mM Tris–HCl, 150 mM NaCl, 1 mM $CaCl_2$, 1 mM $MgCl_2$, 2 mM $MnCl_2$, 10 mM Hepes, pH 7.4) completed with 5 mg ml^{-1} BSA; USPIO$_{COOH}$-NSP-PEG was used as a negative control compound. The nanoparticles bound to the tissue were stained 30 min with Perls's working solution (mixing equal volumes of 5% potassium ferrocyanide and 2% HCl). After rinsing four times for 5 min in distilled water and one time for 5 min in tap water, the tissue was stained 10 min with 0.05% DAB completed with 0.02% H_2O_2 in PBS. The sections were finally counterstained with hemalun and Luxol fast blue and mounted in a permanent medium.

4.7.2.2 Immunohistochemistry: Histological samples were rehydrated and endogenous peroxidases were then blocked with 0.15% H_2O_2, while endogenous biotin was blocked with a blocking kit (Invitrogen). VCAM-1 expression was identified by overnight incubation with 2 μg ml^{-1} of rabbit anti-VCAM-1 polyclonal antibody (Santa Cruz Biotechnology, Heidelberg, Germany), followed by 1 h incubation with 10 μg ml^{-1} of biotinylated goat anti-rabbit IgG (Vector Labconsult) and streptavidin-linked peroxydase complexes (ABC kit, DakoCytomation). Subsequently, the sections were incubated for 5 min with 50 mM Tris–HCl, pH 7.4, and then stained with 0.05% DAB completed with 0.02% H_2O_2 in PBS. The sections were finally counterstained as described above.

Acknowledgements

This work was financially supported by the ARC (research contract nos 00/05-258 and 05/10-335), NOMADE, FRIA, FNRS, ENCITE and TELEVIE (grant number 7.4547.08) Programs of Research of the French Community of Belgium, and it was performed in the framework of COST D38 (Metal-Based Systems for Molecular Imaging Applications) and the European Network of Excellence EMIL (European Molecular Imaging Laboratories) program LSCH-2004-503569. The authors thank Mrs Annik Maes for her technical assistance in immunohistochemistry studies.

References

1. Burtea C, Laurent S, Vander Elst L, Muller RN. Contrast agents – magnetic resonance. In Handbook of Experimental Pharmacology, Semmler W, Schwaiger M (eds). Springer: Berlin, 2008; 135–165.
2. Corot C, Robert P, Idée JM, Port M. Recent advances in iron oxide nanocrystal technology for medical imaging. Adv Drug Deliv Rev 2006; 58: 1471–1504.
3. Sosnovik DE, Weissleder R. Emerging concepts in molecular MRI. Curr Opin Biotechnol 2007; 18: 4–10.
4. Yang L, Peng XH, Wang YA, Wang X, Cao Z, Ni C, Karna P, Zhang X, Wood WC, Gao X, Nie S, Mao H. Receptor-targeted nanoparticles for in vivo imaging of breast cancer. Clin Cancer Res 2009; 15: 4722–4732.
5. Bulte JWM, Modo MMJ. Introduction: The emergence of nanoparticles as imaging platform in biomedicine. In Nanoparticles in Biomedical Imaging, Bulte JWM, Modo MMJ (eds). Springer: New York, 2008; 1–5.
6. Laurent S, Forge D, Port M, Roch A, Robic C, Vander Elst L, Muller RN. Magnetic iron oxide nanoparticles: synthesis, stabilization, vectorization, physicochemical characterizations, and biological applications. Chem Rev 2008; 108: 2064–2110.
7. Boyer C, Whittaker MR, Bulmus V, Liu J, Davis TP. The design and utility of polymer-stabilized iron-oxide nanoparticles for nanomedicine applications. NPG Asia Mater 2010; 2: 23–30.
8. Perez JM, Kaittanis C. Magnetic nanosensors for probing molecular interactions. In Nanoparticles in Biomedical Imaging, Bulte JWM, Modo MMJ (eds). Springer: New York, 2008; 183–197.
9. Perez JM, Josephson L, Weissleder R. Use of magnetic nanoparticles as nanosensors to probe for molecular interactions. Chembiochem 2004; 5: 261–264.
10. Roch A, Muller RN, Gillis P. Theory of proton relaxation induced by superparamagnetic particles. J Chem Phys 1999; 110: 5403–5411.
11. Muller RN, Gillis P, Moiny M, Roch A. Transverse relaxivity of particulate MRI contrast media: from theories to experiments. Magn Reson Med 1991; 222: 178–182.
12. Song Q, Zhang ZJ. Shape control and associated magnetic properties of spinel cobalt ferrite nanocrystals. J Am Chem Soc 2004; 126: 6164–6168.
13. Song Q, Zhang ZJ. Correlation between spin-orbital coupling and the superparamagnetic properties in magnetite and cobalt ferrite spinel nanocrystals. J Phys Chem B 2006; 110: 11205–11209.
14. Bridot JL, Faure AC, Laurent S, Rivière C, Billotey C, Hiba B, Janier M, Josserand V, Coll JL, Elst LV, Muller R, Roux S, Perriat P, Tillement O. Hybrid gadolinium oxide nanoparticles: multimodal contrast agents for in vivo imaging. J Am Chem Soc 2007; 129: 5076–5084.
15. Mornet S, Vasseur S, Grasset F, Duguet E. Magnetic nanoparticle design for medical diagnosis and therapy. J Mater Chem 2004; 14: 2161–2175.
16. Chemla YR, Grossman HL, Poon Y, McDermott R, Stevens R, Alper MD, Clarke J. Ultrasensitive magnetic biosensor for homogeneous immunoassay. Proc Natl Acad Sci USA 2000; 97: 14268–14272.
17. Grossman HL, Myers WR, Vreeland VJ, Bruehl R, Alper MD, Bertozzi CR, Clarke J. Detection of bacteria in suspension by using a superconducting quantum interference device. Proc Natl Acad Sci USA 2004; 101: 129–134.
18. Kriz K, Gehrke J, Kriz D. Advancements toward magneto immunoassays. Biosens Bioelectron 1998; 13: 817–823.
19. Baselt DR, Lee GU, Natesan M, Metzger SW, Sheehan PE, Colton RJ. A biosensor based on magnetoresistance technology. Biosens Bioelectron 1998; 13: 731–739.
20. Edelstein RL, Tamanaha CR, Sheehan PE, Miller MM, Baselt DR, Whitman LJ, Colton RJ. The BARC biosensor applied to the detection of biological warfare agents. Biosens Bioelectron 2000; 14: 805–813.
21. Burtea C, Laurent S, Roch A, Vander Elst L, Muller RN. C-MALISA (Cellular Magnetic-Linked Immunosorbent Assay), a new application of cellular ELISA for MRI. J Inorg Biochem 2005; 99: 1135–1144.
22. Burtea C, Laurent S, Vander Elst L, Muller RN. Highly sensitive streptavidin-based magnetic nanosensors as a useful tool in clinical diagnosis. ESMRMB 2004; e-poster 372; DOI: 10.1594/ESMRMB04/372.
23. Kim GY, Josephson L, Langer R, Cima MJ. Magnetic relaxation switch detection of human chorionic gonadotrophin. Bioconjug Chem 2007; 18: 2024–2028.

24. Colombo M, Ronchi S, Monti D, Corsi F, Trabucchi E, Prosperi D. Femtomolar detection of autoantibodies by magnetic relaxation nanosensors. Anal Biochem 2009; 392: 96–102.
25. Lee H, Sun E, Ham D, Weissleder R. Chip-NMR biosensor for detection and molecular analysis of cells. Nat Med 2008; 14: 869–874.
26. Roch A, Gossuin Y, Muller RN, Gillis P. Superparamagnetic colloid suspensions: water magnetic relaxation and clustering. J Magn Magn Mater 2005; 293: 532–539.
27. Laumonier C, Segers J, Laurent S, Michel A, Coppée F, Belayew A, Elst LV, Muller RN. A new peptidic vector for molecular imaging of apoptosis, identified by phage display technology. J Biomol Screen 2006; 11: 537–545.
28. Burtea C, Laurent S, Lancelot E, Ballet S, Murariu O, Rousseaux O, Port M, Vander Elst L, Corot C, Muller RN. Peptidic targeting of phosphatidylserine for the MRI detection of apoptosis in atherosclerotic plaques. Mol Pharm 2009; 6: 1903–1919.
29. Burtea C, Laurent S, Port M, Lancelot E, Ballet S, Rousseaux O, Toubeau G, Vander Elst L, Corot C, Muller RN. Molecular MRI of VCAM-1 expression in inflammatory lesions using a peptide-vectorized paramagnetic imaging probe. J Med Chem 2009; 52: 4725–4742.
30. Larbanoix L, Burtea C, Laurent S, Van Leuven F, Toubeau G, Vander Elst L, Muller RN. Potential amyloid plaque-specific peptides for the diagnosis of Alzheimer's disease. Neurobiol Aging 2010; 31: 1679–1689. DOI: 10.1016/j.neurobiolaging.2008.09.021.
31. Laumonier C, Laurent S, Roch A, Vander Elst L, Muller RN. Enzymatic titration by relaxometric measurement. 4th Scientific Meeting of the Wallonia Network for Nanotechnologies (NanoWal), ULB, Brussels, 2005.
32. Laumonier C, Laurent S, Roch A, Vander Elst L, Muller RN. Using superparamagnetic particles and relaxometric measurement for enzymatic titration. Workshop on Nanoscience and Nanotechnology, Interreg IIIc, Nancy, France, 2006.
33. Segers J, Laumonier C, Burtea C, Laurent S, Vander Elst L, Muller RN. From phage display to magnetophage, a new tool for magnetic resonance molecular imaging. Bioconjug Chem 2007; 18: 1251–1258.
34. Boutry S, Forge D, Burtea C, Mahieu I, Murariu O, Laurent S, Vander Elst L, Muller RN. How to quantify iron in an aqueous or biological matrix: a technical note. Contrast Media Mol Imag 2009; 4: 299–304.
35. Philibert P, Philibert A, Wang W, Wang A-P, Wang N, Larroque C, Saven JG, Courtête J, Weiss E, Martineau P. A focused antibody library for selecting scFvs expressed at high levels in the cytoplasm. BMC Biotechnol 2007; 7. DOI: 10.1186/1472-6750-7-81.
36. Aravind L, de Souza RF, Iyer LM. Predicted class-I aminoacyl tRNA synthetase-like proteins in non-ribosomal peptide synthesis. Biol Direct 2010; 5. DOI: 10.1186/1745-6150-5-48.
37. Sarikaya M. Biomimetics: Materials fabrication through biology. Proc Natl Acad Sci 1999; 96: 14183–14185.
38. Boutry S, Laurent S, Vander Elst L, Muller RN. Specific E-selectin targeting with a superparamagnetic MRI contrast agent. Contrast Media Mol Imag 2006; 1: 15–22.
39. Port M, Corot C, Raynal I, Rousseaux O. US Patent 2004/0253181 A1.